Lab on a Chip

PAPER

View Article Online
View Journal | View Issue

Cite this: *Lab Chip*, 2016, **16**, 2494

Impedimetric detection and lumped element modelling of a hemagglutination assay in microdroplets†

Merve Marcali and Caglar Elbuken*

Droplet-based microfluidic systems offer tremendous benefits for high throughput biochemical assays. Despite the wide use of electrical detection for microfluidic systems, application of impedimetric sensing for droplet systems is very limited. This is mainly due to the insulating oil-based continuous phase used for most aqueous samples of interest. We present modelling and experimental verification of impedimetric detection of hemagglutination in microdroplets. We have detected agglutinated red blood cells in microdroplets and screened whole blood samples for multiple antibody sera using conventional microelectrodes. We were able to form antibody and whole blood microdroplets in PDMS microchannels without any tedious chemical surface treatment. Following the injection of a blood sample into antibody droplets, we have detected the agglutination-positive and negative droplets in an automated manner. In order to understand the characteristics of impedimetric detection inside microdroplets, we have developed the lumped electrical circuit equivalent of an impedimetric droplet content detection system. The empirical lumped element values are in accordance with similar models developed for single phase electrical impedance spectroscopy systems. The presented approach is of interest for label-free, quantitative analysis of droplets. In addition, the standard electronic equipment used for detection allows miniaturized detection circuitries that can be integrated with a fluidic system for a quantitative microdroplet-based hemagglutination assay that is conventionally performed in well plates.

Received 12th May 2016,
Accepted 23rd May 2016

DOI: 10.1039/c6lc00623j

www.rsc.org/loc

Introduction

Microdroplet-based microfluidic systems have enabled a range of applications in biochemical analysis.[1–3] The ability to compartmentalize individual cells or specific concentrations of biochemical entities opens up a plethora of applications for these systems.[4] In parallel with the developments in high throughput droplet generation and several other droplet operations such as merging, mixing, splitting, and reinjection, these systems can collect significant statistical data in short assay times. Although several interesting droplet operation units have been demonstrated with microdroplets, there is still lack of standard modelling methods that can be applied to microdroplet-based detection.

Impedimetric methods are commonly used for sensing in microfluidic systems. Detection of cells with impedimetric measurement dates back to the seminal works of Curtis and Cole.[5–7] The Coulter method was developed as a standard tool that has been used for cytometry devices for decades.[8] There has been tremendous progress ever since especially for identification of single cells based on their electrical properties.[9–11] With the advancements in microdroplet-based fluidic systems, impedimetric detection of the content of microdroplets has also been discussed.[12–14] Specifically, there have been several applications that encapsulate cells in droplets.[15,16] Detection of these cells has mostly been performed using optical methods since the commonly used oil-based continuous phase liquids have very high impedances and pose challenges for electrical detection. The thin oil lubrication layer between an aqueous droplet and the channel wall is the main limitation for the use of impedimetric methods in detection of cells in droplets. Recently, it has been demonstrated that viable mouse myeloma cells (5–6 μm diameter) can be detected inside microdroplets using some advanced detection systems and conductivity adjusted solutions.[17] However, the signal-to-noise ratio was limited and the system can only detect viable cells in low conductivity buffers. There is still need for systems that can be used for impedimetric detection using real-world samples. Also, there is a gap in the literature for modelling of impedimetric detection inside microdroplets.

UNAM, Institute of Materials Science and Nanotechnology, Bilkent University, Ankara, 06800, Turkey. E-mail: elbuken@unam.bilkent.edu.tr

† Electronic supplementary information (ESI) available. See DOI: 10.1039/c6lc00623j

In the present article, we have demonstrated the first impedimetric detection of hemagglutination inside microdroplets. We explore the detection of clumps of cells and development of a lumped model analysis for detection of cellular aggregation inside microdroplets. In contrast to the previously reported lumped models of impedimetric detection, we present empirical values for the lumped model elements. In our system, each microdroplet can be used to detect a separate agglutination reaction. This approach enables cross screening of multiple samples for various analytes using a single system.

We developed a PDMS microfluidic device to generate a train of serum droplets containing agglutinins. Then, a PBS (phosphate-buffered saline) diluted whole blood sample is injected into these droplets from a side inlet. As a model assay, we have demonstrated agglutination of red blood cells (RBCs) by antibodies in serum using standard blood typing sera.[18] Blood typing sera are readily accessible and provide a very easy assay to test impedimetric detection of agglutinated and non-agglutinated droplets using microfabricated electrodes. We have demonstrated that using this label-free and automated impedimetric detection approach, hemagglutination inside the droplets can be monitored. By analyzing the impedimetric signal of droplets with different contents, we have developed the lumped electrical circuit equivalent of the microfluidic detection system. Using SPICE circuit simulator software, the lumped model elements were derived from the experimental values. This final model provides us with an electrical circuit equivalent of microdroplet sensors that can be integrated with control and read-out electronics for stand-alone lab on a chip systems. By correlating the physical parameters to the individual elements of the model, such a model can be applied for designing quantitative immuno-diagnostic assays in microdroplets[19] or can be further expanded to model the detection of individual cells in microdroplets.[17]

In this article, we first describe the microfluidic chip design and its fabrication. Formation of serum droplets with whole blood side injection was demonstrated without any chemical treatment of the PDMS/glass microchips. Secondly, we discuss the experimental measurement system, followed by the impedimetric sensing results. We have demonstrated the repeatability and the limit of detection of the system. Then, the lumped circuit model for the microdroplet system is introduced. Finally, the SPICE circuit model is used to determine the values of the circuit components and comparison of the numerical model and the experimental results is given. The results in this study demonstrate the impedimetric detection of hemagglutination in microdroplets, which shows the feasibility of a completely automated hemagglutination assay performed in a microfluidic format using an integrated antibody dilution unit. Conventionally such assays are performed using well plates and require serial dilutions of the test solutions (virus, bacteria or antibody) as well as manual tracking and reading of the agglutinated wells.

Experimental section

Materials

We obtained whole blood samples from adult donors with written consent. Blood samples (A+, AB+, and O−) were drawn into a 4 ml tube (BD Vacutainer) containing EDTA (ethylenediaminetetraacetic acid) and stored at 4 °C. For each experiment, 1 ml of a whole blood sample was diluted to a total volume of 3 ml with PBS solution (Sigma). Antibody sera (IgM Anti-A, Anti-B, Anti-D) were obtained from a local store (Agape Diagnostics). Silicone oil (μ = 100 mPa s, Ultrakim) was used as a continuous phase to form microdroplets.

Device fabrication

Microfluidic device fabrication was accomplished in two steps. Firstly, we fabricated PDMS (Sylgard 184, Dow Corning) microchannels using standard soft lithography.[20] A silicon wafer (University Wafers) was used as a substrate on which SU-8 negative photoresist (MicroChemicals) was patterned using photolithography. Then, for the casting process, we prepared a PDMS (polydimethylsiloxane) mixture. The mixture was cured on the silicon mold at 100 °C for 4 h. The microchannel height and width were measured to be 80 μm and 300 μm, respectively, using a stylus profilometer (KLA Tencor, P6 Surface Profiler). Secondly, coplanar electrodes were fabricated on a glass slide. AZ5214 positive photoresist (MicroChemicals) was patterned on a glass slide using photolithography. The glass slide was coated with a 15 nm-thick Cr and a 35 nm-thick Au using a thermal evaporator (Vaksis-PVD Vapor-3S). Electrode fabrication was completed by a lift-off process in acetone (Sigma). The electrode width and gap were measured to be 20 μm. Finally, a microchannel was bonded over the coplanar electrodes using an oxygen plasma treatment (Nanoplas, DSB6000). After plasma bonding, we have not performed any surface modification. We simply filled the device with silicone oil and placed it on a hotplate at 100 °C overnight. We have observed that overnight baking enhances the hydrophobic nature of the channel.

Device design and droplet formation

We designed a microfluidic chip that allows screening of a whole blood sample with multiple antibody serum solutions in a single run. The chip design and measurement setup are schematically shown in Fig. 1. A T-junction droplet generator is used in a squeezing regime[21] to form antibody serum droplets using silicone oil as a continuous phase. Then, using an additional side injection channel, 6–8 nl of a blood sample is injected into the serum droplets. The control of flow rates was achieved using a pressure pump (Elveflow, OB1, 2 bar). For the results demonstrated in this study, we tested each sample with three antibody solutions (Anti-A, Anti-B, Anti-D) in a single run. The antibody solutions, separated by silicone oil segments, were loaded into PTFE (polytetrafluoroethylene) tubing (Cole Parmer, ID 0.42 mm, OD

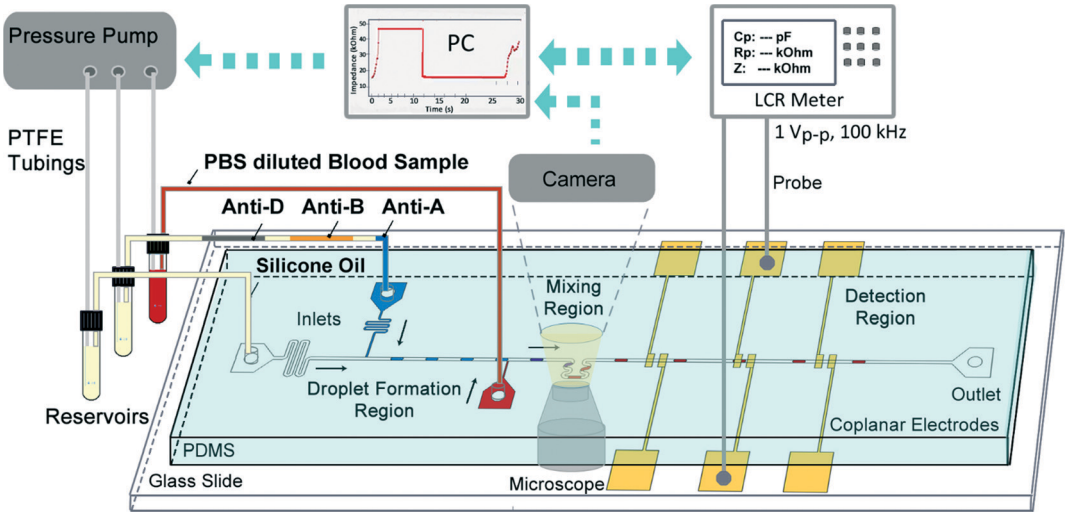

Fig. 1 Schematic of the measurement setup that detects the agglutination reaction inside droplets impedimetrically. Silicone oil is used to generate antibody serum droplets. A 1 : 2 PBS diluted whole blood sample solution is injected into the droplets from the third inlet. Coplanar electrodes and an LCR meter are used for impedimetric detection. Measurement results and microdroplets are monitored in real-time through a computer interface.

0.84 mm) using a syringe pump (KD Scientific, KDS200) in withdraw mode. Segmentation of the antibody solutions prevented cross contamination of reagents in the tubing. For effective antigen–antibody binding after side injection, microdroplets are mixed using a serpentine channel segment. Finally, the agglutination reaction inside the microdroplet is detected using coplanar electrodes and an LCR meter.

It is important to emphasize that we have not used any surface modification or surfactant when forming microdroplets of the serum–whole blood mixture. The main challenge in dealing with whole blood in two-phase flow systems is the wetting of blood droplets in polymer microdevices. Several groups have tackled this problem.[22,23] Ismagilov *et al.* have modified the surface of a PDMS channel in order to prevent cell adhesion. This modification requires a tedious

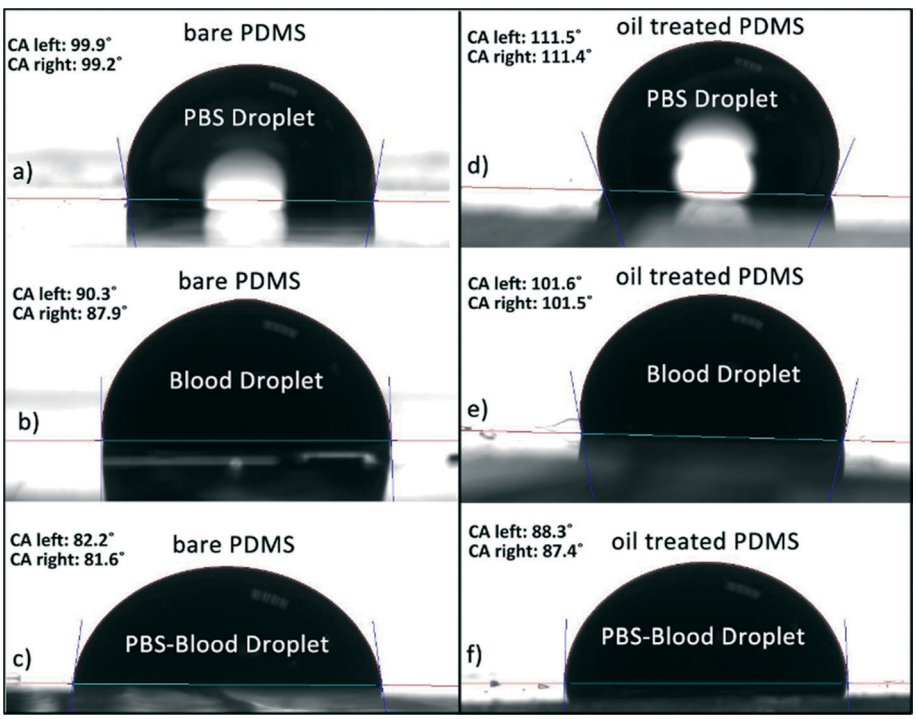

Fig. 2 Contact angle measurement results for bare (a, b, c) and oil treated PDMS (d, e, f). Oil treatment increases the contact angle for all three scenarios: a PBS droplet (a and d), a whole blood droplet (b and e) and a 2 : 1 v/v PBS : whole blood droplet (c and f).

silanization procedure. We overcame the protein adsorption issue simply by treating the microchip with silicone oil for a duration of at least 10 h. During this incubation step, silicone oil is absorbed by the porous PDMS which enhances the hydrophobicity of the channel walls. Fig. 2 demonstrates our contact angle measurement (OCA 30, Dataphysics) results obtained from bare PDMS and oil treated PDMS. As seen in Fig. 2b–e, the contact angle for whole blood increases from 89° to 101° for the PDMS surfaces that had absorbed oil for at least 10 h. Similarly for the 1 : 2 (v/v) blood–PBS droplet mixtures, the contact angle increases from 82° to 88° (Fig. 2c–f).

In order to form the droplets, the inlet pressures were set to 45 mbar and 50 mbar for the antibody solution and silicone oil inlets, respectively. After successful droplet formation was observed at a rate of 0.1 Hz, the inlet pressure for the whole blood sample is gradually increased up to 42 mbar. The time lapse snapshots of injection of the blood sample into an Anti-A droplet are shown in Fig. 3a–c. A short movie of the injection of the whole blood sample into serum droplets is also given as ESI† (Video S1). The pressure control system allowed us to fine tune the inlet pressures for synchronous injection of whole blood into the droplets. The system can operate without any operator interruption for more than 60 min, thus allowing analysis of multiple droplets in a successive manner. The PBS diluted whole blood in the vial was mixed using a magnetic stirrer throughout the course of the experiment in order to prevent erythrocyte sedimentation.

In the literature, there are several droplet microfluidic systems that demonstrate synchronous formation of droplets using multiple dispersed phase solutions.[24–26] In general, these systems are self-triggered to form droplets from multiple junctions. In our system, the whole blood sample introduced at the downstream T-junction does not form a complete droplet. Instead, as it is in the filling stage, a serum antibody droplet merges with it and the combined droplet goes through the necking stage.[27] Synchronization in merging of droplets was achieved precisely and the experiment ran more than 60 min without requiring any pressure adjustment by the operator.

The combined droplets were directed to a serpentine region for mixing. At the end of the serpentine channel, the red blood cells, which were mixed with the corresponding antibody solutions, started to separate from the plasma and accumulated at the trailing edge of the droplets. Agglutination of RBCs in the serpentine region is shown in the second movie supplemented as ESI† (Video S2). In this video, agglutination-positive droplets are separated from whole blood droplets. During the mixing step, individual RBCs started to bind with one another due to the reaction of agglutinogens on RBCs with antibodies in the serum solution and formed RBC clusters in a droplet. The accumulation of the RBC clusters at the trailing edge is due to the recirculative flow profiles formed in the droplet. The microdroplets in rectangular channels possess a complex profile of flow patterns which depend on the droplet velocity, viscosity ratio of the fluids and surface tension.[28,29] As recently demonstrated, depending on the sedimentation rate of the particles inside the droplets and the length of the droplet, nonagglutinated RBCs may also partially accumulate at the trailing edge of the droplet.[30] In our studies, we ensured that the Ca number is high enough so that the nonagglutinated RBCs stay homogenously suspended in the droplet ($Ca = \mu U/\gamma = (100\ mPa\ s \times 150 \times 10^{-6}\ m\ s^{-1})/4 \times 10^{-3}\ N\ m^{-1} = 3.75 \times 10^{-3}$). The critical capillary number for the homogenous mixing regime is determined to be 2.3×10^{-3} for 500 μm long droplets. Additionally, the length of the serpentine section was designed as 9 mm so that each droplet has a reaction time of 2 min before reaching the detection electrode.

It is also important to note that at the side injection T-junction, an antibody droplet merges with whole blood from the leading edge (ESI† Video S1). Right after the merging as

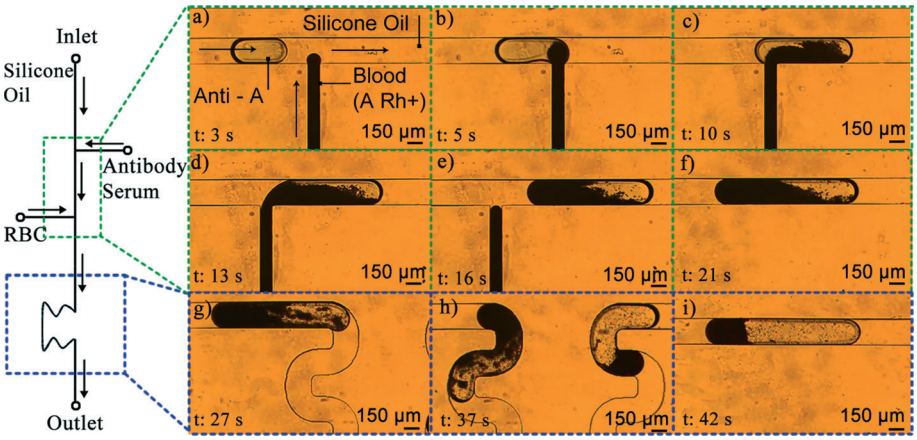

Fig. 3 Schematic drawing of the system and time-lapse optical micrographs of sample side injection into the droplets. (a) At the first T-junction, an antibody (Anti-A) droplet is generated. (b–d) The droplet is merged with a blood sample (A Rh+). (e and f) The droplet is transferred to the mixing region. (g and h) Mixing of the antibody solution with the blood sample to enhance hemagglutination. (i) After agglutination, clumped red blood cells are located at the trailing edge of the droplet.

the droplet moves in the channel, the RBCs slowly coast towards the trailing edge while the antibody solution moves to the leading edge of the droplet. This provides an effective mechanism for the agglutinogens on RBCs to meet with agglutinins in the serum. As seen in the second supplementary movie (ESI† Video S2), even at the entrance of the serpentine region, the hemagglutination reaction has started and clumps of RBCs can be distinguished. Therefore, the side injection of the blood sample and the well-known serpentine mixing geometry enable efficient binding and eliminate the need for active mixers used in the literature.[19]

Measurement setup

In previous studies, for an impedimetric measurement, custom-made electronics, lock-in amplifiers and LCR meters were used in microfluidics systems.[31,32] In this study, we used an LCR meter (Agilent E4980A) to observe the agglutination reaction inside microdroplets and to characterize the signal obtained from different droplets. The whole blood sample is mixed with three types of antibody serum (Anti-A, Anti-B, Anti-D) as explained in the previous section. Due to ease of fabrication, we used coplanar electrodes for detection. The electrodes were supplied a sinusoidal signal of 1 V_{p-p} amplitude by the LCR meter. The excitation frequency was swept from 50 kHz to 2 MHz and measurements were performed in $|Z| - \theta$ mode. The 100 kHz frequency yielded the best signal (largest difference between the agglutinated and non-agglutinated sections of the droplet) for the detection of the agglutination-positive droplets, thus a further detailed investigation of the system was performed at 100 kHz. Although an LCR meter is a very precise instrument for electrical characterization, it is limited in terms of its data rate. The measurement time (from trigger to end of measurement) for an Agilent E4980A is reported to be 5.7 ms in its data sheet. In order to reach this limit, we set the measurement time mode as short and kept the LCR display off. With these settings we were able to acquire data at 135 Hz. We used a custom LabVIEW interface to transfer the experimental readings to a computer in real-time. Simultaneously, the system was also monitored using an inverted microscope (Omano OMFL600) equipped with a 5 MP camera.

Results and discussion

In this study our goal is to detect agglutination reactions inside microdroplets using electrical sensing. We also aimed to develop an electrical equivalent circuit model for impedimetric detection inside water-in-oil microdroplets. We designed a droplet based microdevice that merged whole blood with antibody serum droplets in silicone oil. For impedimetric measurement, firstly, droplets that contained whole blood and different types of antibody serum were formed. Then, an electrical signal was recorded as droplets travelled over the coplanar electrodes. Since the conductivity of the droplets is significantly higher than silicone oil, the droplets were detected as low impedance signals. As shown in Fig. 4, the continuous phase impedance was on the order of MΩ, whereas impedance of reagents in the droplets was on the order of kΩ for the measurements performed at 100 kHz. Fig. 4 shows four different droplet types that have been characterized in a single run. Blood droplets and antibody droplets can be differentiated from their impedance peak. A blood sample has an impedance of 13.5 kΩ, whereas an antigen droplet yields 9.1 kΩ. Since very narrow electrodes were used, when the sensing region is completely occupied by the droplet, the signal saturates at its minimum point. Then, agglutination-positive and agglutination-negative droplets were formed and characterized. When the A+ blood sample is mixed with the Anti-A serum, hemagglutination is observed. The agglutinated RBCs were detected impedimetrically as a clump that gave a characteristic signal at 30 kΩ (also shown in the ESI† Video S3). The leading edge of the droplet is composed of a conductive antigen solution and plasma. As expected, this section yielded a similar impedance result to the conductive droplets. When the A+ blood sample is merged with an Anti-B serum droplet, agglutination was not observed and impedance was detected similar to the homogenously distributed droplets.

For the detailed investigation of the signal from the agglutinated droplet, the droplets were observed at high magnification while the real-time impedance signal is recorded. As shown in Fig. 4, when a droplet enters the sensing region, the signal level drops to 10 kΩ and remains constant between 22 s and 25 s. As the cell clusters enter the sensor, impedance starts to increase due to the insulative nature of the cell membrane (25–27 s) at 100 kHz. The trailing edge of the droplet contains large clusters of cells separated with cell-depleted, plasma-rich portions. The distinct impedance signal observed between 27 s and 28 s is when the plasma-rich portion enters the sensing domain. This causes a sudden decrease in the impedance as shown in Fig. 4. Such a behavior is not observed in non-agglutinated droplets, since RBCs are distributed in the entire droplet. Although there are small clusters of red blood cells, the sensor averages the signal in the entire width of the channel and a constant impedance signal is observed.

Effect of excitation voltage on the impedance signal

In order to test the dependence of the impedance signal on the excitation voltage, the same measurements were performed at different bias signals. A train of agglutination-positive droplets was formed and measured by the same pair of electrodes sequentially. The first droplet was detected using a 1 V_{p-p} signal. For the following droplets, the signal was obtained with increasing signal amplitudes. Fig. 5 plots the signal obtained using 1 V_{p-p} and 10 V_{p-p}, which shows a significant difference. Although both signals detected the narrow agglutinated section at the trailing edge of the droplet, the signal obtained from the droplet body is very different. For the 1 V_{p-p} signal, a constant

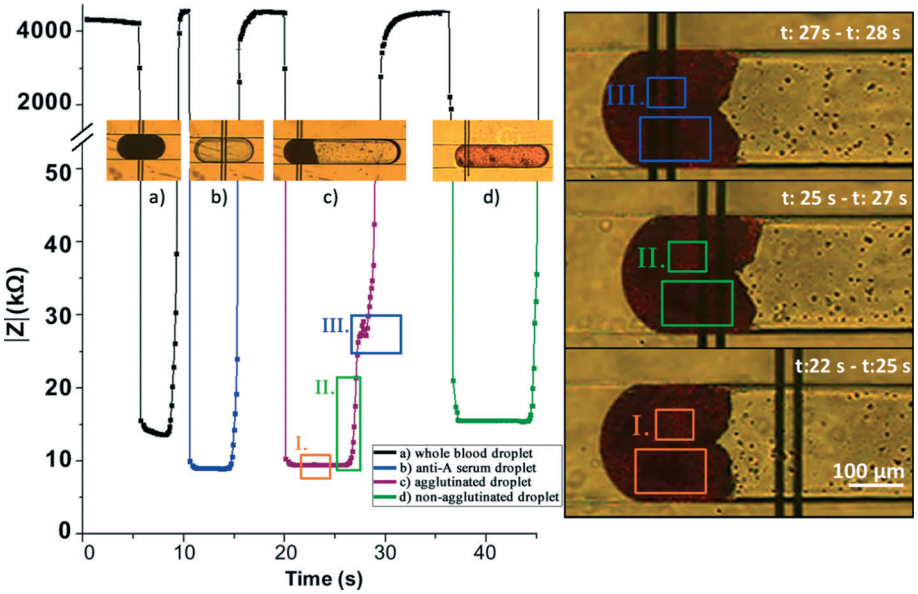

Fig. 4 Impedance signal obtained from different droplets. (a) A whole blood droplet (black). (b) An anti-A antigen droplet (blue). c) An anti-A solution and blood sample (A Rh+) droplet (red). The agglutination reaction occurred inside a droplet. d) An anti-B solution and blood sample (A Rh+) droplet (green). Agglutination did not occur due to the mismatch of the antigen and the antibody. On the right, high magnification optical microscopy image and characteristic impedance signal of the agglutination-positive droplet: I. impedance of the plasma section in the droplet, *t*: 22–25 s (red); II. impedance increase due to the presence of the cells in a droplet, *t*: 25–27 s (green); and III. impedance peak due to the replacement of a red blood cell cluster with a plasma solution, *t*: 27–28 s (blue).

signal level is observed, whereas when 10 V_{p-p} is applied, the impedance gradually increases as the droplet goes over the sensor. The observation of these droplets under the microscope revealed that the freely moving cells in the droplet are trapped by the electrodes due to dielectrophoretic force and the trapping causes an increase in the impedance signal. As the droplet moves, the electrodes sweep the non-agglutinated cells. This squeegee-like behaviour causes an exponential increase in the signal level. Such an effect can be used to transfer particles between successive droplets.

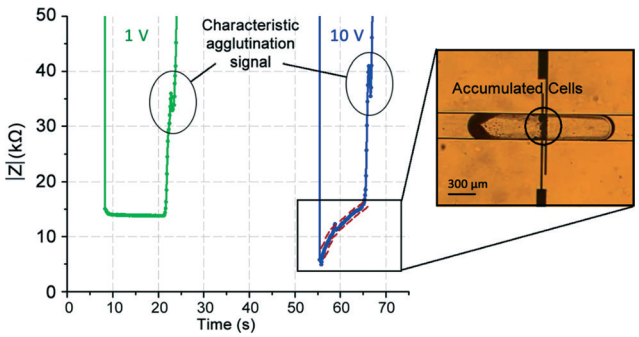

Fig. 5 The effect of excitation voltage on the impedance signal. The plot shows two impedance signal results obtained from agglutination-positive droplets using 1 V_{p-p} and 10 V_{p-p} excitation voltages. The inset shows a microscopy image of the sweeping of free-flowing cells inside the droplets resulting in an increase in the impedance signal. The characteristic agglutination peak is easily distinguished for both voltage levels.

Limit of detection and repeatability

Hemagglutination assays that are conventionally performed in well plates require dilution of the test solution and mixing with the sample in separate wells. After a certain incubation time, the agglutination-positive (pellet) and agglutination-negative (button) wells are read and the quantity of the analyte of interest is determined.[33] As a step towards a hemagglutination assay in microdroplets, we present the impedimetric detection in this study. We also determined the limit of detection by diluting the RBC amount inside the droplets and characterized the repeatability of the system.

In order to determine the limit of detection (LOD), we tailored the inlet pressures and generated microdroplets with a decreasing amount of red blood cells. The amount of dilution was approximated from the microscopy images of red blood cell laden microdroplets. Droplets containing four different dilutions and the corresponding impedance signals are shown in Fig. 6. We can detect the agglutination signal for 2-fold, 4-fold and 12-fold dilutions. For the 15-fold diluted sample, the agglutination signal was barely noticeable. Therefore, we conclude that for the presented system, the LOD is 15-fold dilution of the sample. Narrowing the width of the microchannel in the detection region will elongate the microdroplet and the clumped red blood cells so that decreasing amounts of red blood cells can be detected which would improve the LOD. As seen in Fig. 6, an increase in the dilution rate decreases the impedance value for the characteristic signal, which is due to the increasing amount of PBS inside the droplets.

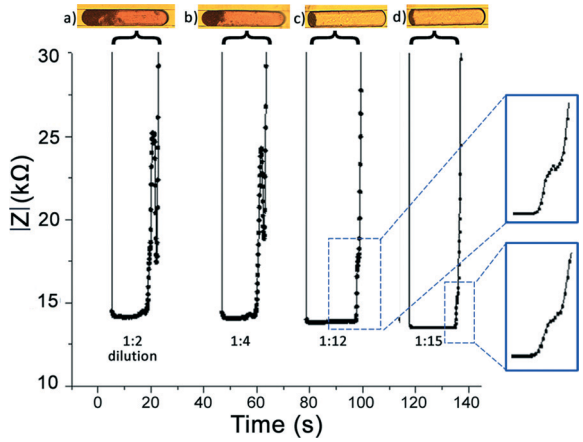

Fig. 6 The impedance signal and optical microscopy images for agglutination-positive droplets (Anti-A solution and A Rh+ blood sample) obtained at four different dilution rates: a) 1 : 2, b) 1 : 4, c) 1 : 12, and d) 1 : 15. The two insets show the signal obtained for the 1 : 12 and 1 : 15 diluted samples which yield the limit of detection for the presented system.

As a metric to evaluate the system's repeatability, we have selected the characteristic impedance plateau that occurs around 30 kΩ for hemagglutination-positive droplets. We analyzed the impedance value for the agglutination-positive droplets for two different microfluidic devices tested on different days. The impedance value corresponding to the characteristic agglutination peaks is plotted in Fig. 7. The intra-assay and inter-assay impedance signals are very similar and vary around 31 kΩ and 26 kΩ for chip 1 and chip 2, respectively.

Impedance model of cells inside a droplet

The main approach in the analytical modelling of impedance cytometry systems was based on the dielectric properties of the medium and the particles of interest.[34] For microfluidic flow cytometry studies, impedance spectroscopy has been investigated in detail.[35] In order to perform impedance analysis of a single particle, generally an equivalent circuit design was used which is mentioned as a lumped element model.[10,31] Then, individual circuit elements were calculated based on the material properties. This model can be used to calculate the resultant impedimetric signal at any given frequency. The results are typically given as Bode plots. Using this approach, the electrical characteristic of a single cell in a microfluidic chip has been demonstrated.[36] Recently, a single cell that was encapsulated by a droplet was modelled and detected electrically by Kemna *et al.*[17]

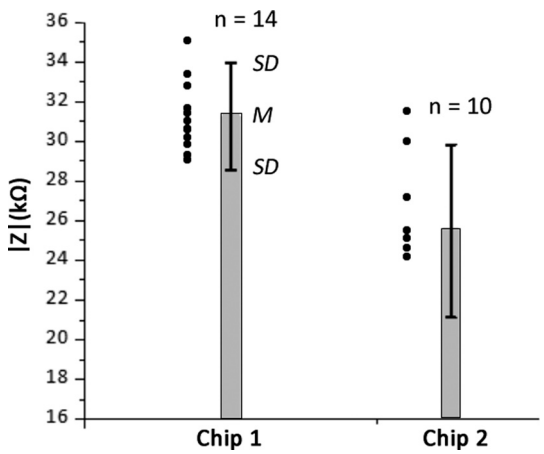

Fig. 7 The impedance value for the agglutinated red blood cells obtained from two different devices tested on different days. The mean (M) and standard deviation (SD) of multiple measurements are shown.

In this study, we apply an empirical approach to derive the lumped element model of the impedimetric droplet-based detection system. By using a lumped model, we have derived an equivalent circuit model from our experimental observations to investigate the electrical properties of agglutination of RBCs in a droplet. Similar models have been given by several other studies; however, the values for the discrete elements are usually not provided.[13,17,37] Lumped element models for detection of single cells in flow cytometry systems[36] and evaporating microdroplets on coplanar electrodes[38] are well developed. However, modelling of cell carrying droplets for a two-phase flow system is a much challenging case for a purely analytical approach. Therefore, we aimed to determine the values of the lumped element parameters using an empirical approach. Finally, the obtained results are compared with the literature.

The lumped element model is shown in Fig. 8. This model incorporates the electrical double layer capacitance (C_{dl}), membrane capacitance of the droplet (C_{mem}), the probe capacitance (C_{probe}) and inductance (L_{probe}). For the droplets, depending on the content, a resistor and capacitor pair was used for the equivalent modelling. As seen in Fig. 8, several different R and C pairs are formed to be determined by the numerical model, *e.g.* resistance of PBS diluted whole blood (R_{blood}), the antibody solution (R_{anti}) and capacitance of PBS diluted whole blood (C_{blood}) and the antibody solution (C_{anti}).

In order to obtain the values of circuit components, first, the experimental data were recorded. By sweeping the applied frequency from 50 kHz to 2 MHz with a constant excitation voltage of 1 V_{p-p}, we examined the signal obtained from four different droplets: a whole blood droplet, an antibody serum droplet, an agglutination-positive droplet and an agglutination-negative droplet. Then, the equivalent lumped element model was introduced in LTspice, which is a SPICE simulator software program to obtain the impedance spectrum of the circuit. A sample numerical impedance spectrum result for the antibody serum droplet is shown in the ESI.† The lumped model for each of the scenarios shown in Fig. 8 was formed in the SPICE simulator environment. Then, the values for the circuit elements were iteratively changed, until the simulated impedance spectrum converged with the experimental results. Starting from the simplest case, *i.e.* the open circuit impedance of the detection system with probes, we

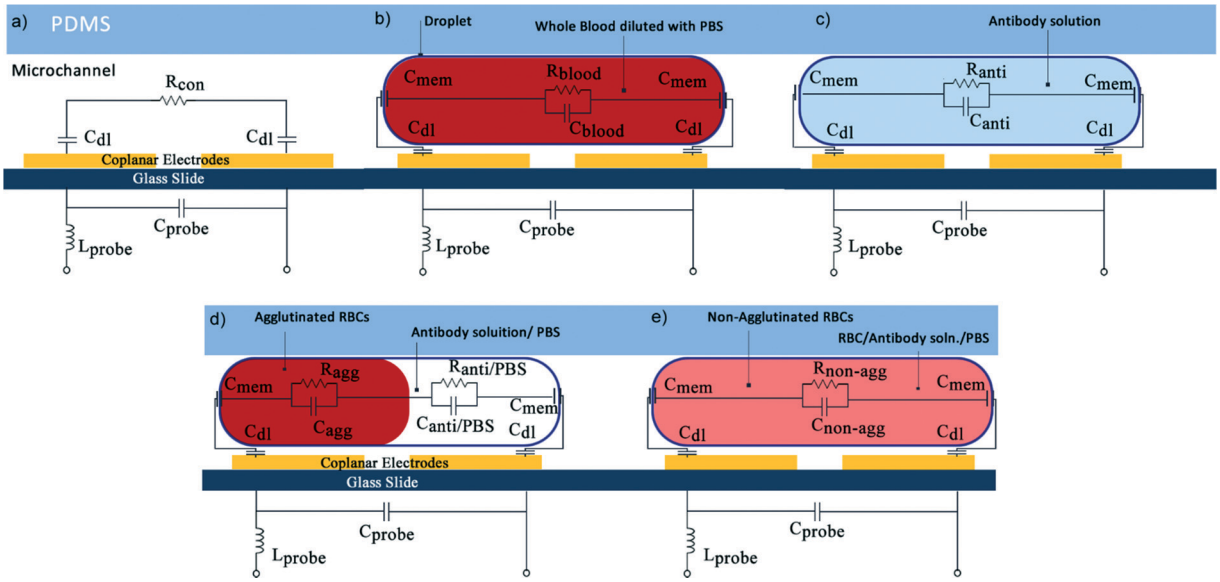

Fig. 8 Equivalent circuit model of the system for five scenarios: a) the continuous phase fluid over the electrodes (*i.e.* no droplet), b) a whole blood droplet diluted with PBS, c) an antibody solution droplet, d) an agglutination-positive droplet, and e) an agglutination-negative droplet. The experimental results for each of these five cases can be seen in Fig. 5.

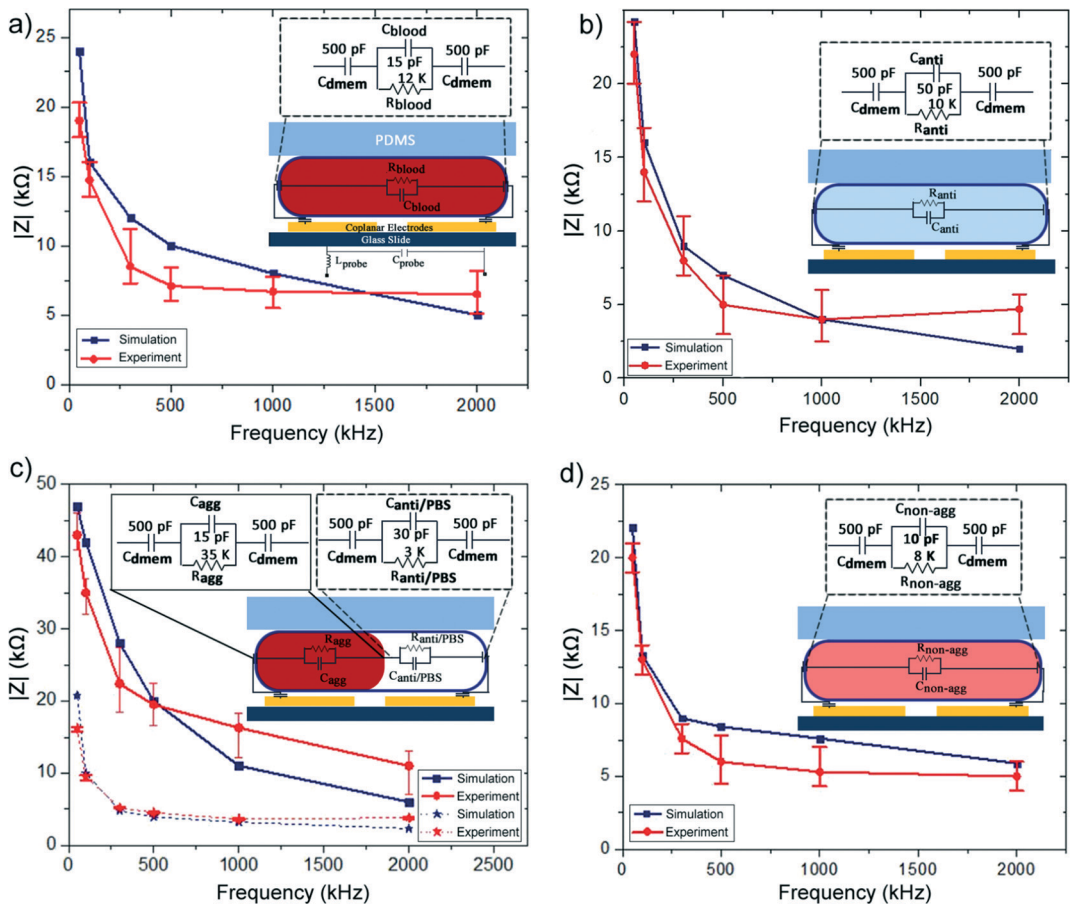

Fig. 9 Bode plots obtained from the experiments performed at six different frequencies (n = 3) and the equivalent circuit simulations: a) a PBS diluted whole blood droplet, b) an antibody solution droplet, c) an agglutination-positive droplet, and d) an agglutination-negative droplet.

obtained the experimental results and determined the circuit element values that fit the experimental results. First, we have found that the probe can be modelled with serial inductor and parallel capacitance values of 780 nH and 150 fF, respectively. Then, incrementally we have improved the lumped model to include the elements describing the microfluidic system. Starting from the simplest scenario, we sequentially formed the complete model. We determined the resistance of the continuous phase R_{con} to be 10 MΩ. It is important to note that for any given experimental data the values for the electrical circuit model that converge with the experimental data may not be unique. In order to have a unique solution set, the measurements have been performed at six different frequencies. The frequency range was selected so that the capacitive and inductive components change in order of magnitude throughout the scanned spectrum. This allowed us to observe the real and imaginary parts of the impedance signal to find the individual R, C and L values.

The experimental values and the output of the numerical SPICE model are summarized in Fig. 9 for signals obtained from different droplets. The experimental results are averaged values of three measurements whereas the error bars show the minimum and the maximum values. As a result, the simulated and experimentally observed values were in good agreement.

It is worth noting that impedimetric analysis of particles inside microdroplets has not been performed before. The carrier liquid and additional droplet interface poses challenges in the analytical modelling approaches based on Maxwell's mixture theory.[39] However, the presented empirical approach allows us to determine the individual circuit component values relatively easier. When, the resultant values are investigated, we conclude that the R and C values obtained within the droplet are consistent with the material properties of the bulk solutions. It is interesting to note that the droplet interface introduces an additional 500 pF capacitance to the system similar to the membrane capacitance used for modelling individual cells in a continuous flow. The membrane capacitance for single cells is usually reported in terms of capacitance per unit area, which is on the order of a few mF m^{-2}.[36,40–42] Similarly the droplet membrane capacitance is found to be 1.4 mF m^{-2} in our system. These results demonstrate that dielectric modelling of individual cells inside droplets can be performed with a double shell single core model. As shown in the ESI,† the double layer capacitance of the system was determined to be 800 pF. The electrodes used in our system was 20 μm in width and 300 μm in length with a spacing of 20 μm between two electrodes. The double layer capacitance for these electrodes is also in accordance with the double layer capacitances reported previously.[36] We should note that when we used wider electrodes (50 μm and 100 μm), the signal for agglutination-positive droplets was not as distinct as the ones shown in this study. This is due to the fact that narrowing down the electrodes decreases the measurement volume and allows the analysis of droplets in smaller slices.

Another important component in the lumped element model was the effect of the probe capacitances. We have found that the probes that we have used for our LCR meter measurement system can be modeled as a parallel LC system. This result and the individual values of these elements (780 nH and 150 fF) were also verified by measuring the impedance response of through-hole components mounted on a breadboard. The consideration of the inductive term is especially critical since it increases the overall impedance of the system at high impedance values and should be considered together with the parasitic effects usually considered for hybrid PDMS/glass microfluidic systems.

Conclusion

We have reported a microfluidic device to measure agglutination reactions in microdroplets using a label-free approach. Droplets that included antibody solutions were mixed with a whole blood sample to form hemagglutination in droplets. The formation of agglutinated clusters was detected impedimetrically using conventional microfabricated electrodes. An equivalent lumped-element model of the system is derived from the experimentally measured parameters. The presented device provides a method that allows screening of samples against multiple analytes for automated agglutination-based assays. This study also demonstrates a whole blood-based assay in PDMS microfluidic channels without any tedious surface treatment. The impedimetric results were obtained using standard solutions and whole blood. This system does not require any specific buffers or any sample preparation for conductivity adjustment which in turn makes this method a candidate for an automated hemagglutination system which operates with nanoliter volume of samples.

Acknowledgements

We gratefully acknowledge support from the European Union FP7 Marie Curie Career Integration Grant (no. 322019).

References

1 H. N. Joensson and H. Andersson-Svahn, *Lab Chip*, 2011, **11**, 4144–4147.
2 L. Rosenfeld, T. Lin, R. Derda and S. K. Tang, *Microfluid. Nanofluid.*, 2014, **16**, 921–939.
3 A. B. Theberge, F. Courtois, Y. Schaerli, M. Fischlechner, C. Abell, F. Hollfelder and W. T. Huck, *Angew. Chem., Int. Ed.*, 2010, **49**, 5846–5868.
4 Y. Zhu and Q. Fang, *Anal. Chim. Acta*, 2013, **787**, 24–35.
5 K. S. Cole and H. J. Curtis, *J. Gen. Physiol.*, 1939, **22**, 649–670.
6 K. S. Cole and H. J. Curtis, *J. Gen. Physiol.*, 1941, **24**, 551–563.
7 H. J. Curtis and K. S. Cole, *J. Gen. Physiol.*, 1937, **21**, 189–201.

8 W. H. Coulter, *US Pat.*, 2656508, 1953.
9 S. Gawad, K. Cheung, U. Seger, A. Bertsch and P. Renaud, *Lab Chip*, 2004, **4**, 241–251.
10 S. Gawad, L. Schild and P. Renaud, *Lab Chip*, 2001, **1**, 76–82.
11 D. Holmes, D. Pettigrew, C. H. Reccius, J. D. Gwyer, C. van Berkel, J. Holloway, D. E. Davies and H. Morgan, *Lab Chip*, 2009, **9**, 2881–2889.
12 P. K. Isgor, M. Marcali, M. Keser and C. Elbuken, *Sens. Actuators, B*, 2015, **210**, 669–675.
13 J. Janouš, J. Čech, P. Beránek, M. Přibyl and D. Šnita, *J. Micromech. Microeng.*, 2013, **24**, 015002.
14 A. P. Lee, J. Lopez-Prieto, R. Lin and M. Simon, *US Pat.*, 20150322487, 2015.
15 S. Köster, F. E. Angile, H. Duan, J. J. Agresti, A. Wintner, C. Schmitz, A. C. Rowat, C. A. Merten, D. Pisignano and A. D. Griffiths, *Lab Chip*, 2008, **8**, 1110–1115.
16 Y. J. Sung, J. Y. H. Kim, K. W. Bong and S. J. Sim, *Analyst*, 2016, **141**, 989–998.
17 E. W. Kemna, L. I. Segerink, F. Wolbers, I. Vermes and A. van den Berg, *Analyst*, 2013, **138**, 4585–4592.
18 S. Makulska, S. Jakiela and P. Garstecki, *Lab Chip*, 2013, **13**, 2796–2801.
19 B. Teste, A. Ali-Cherif, J. L. Viovy and L. Malaquin, *Lab Chip*, 2013, **13**, 2344–2349.
20 D. C. Duffy, J. C. McDonald, O. J. Schueller and G. M. Whitesides, *Anal. Chem.*, 1998, **70**, 4974–4984.
21 G. F. Christopher and S. L. Anna, *J. Phys. D: Appl. Phys.*, 2007, **40**, R319.
22 T. R. Kline, M. K. Runyon, M. Pothiawala and R. F. Ismagilov, *Anal. Chem.*, 2008, **80**, 6190–6197.
23 B. Subramanian, N. Kim, W. Lee, D. A. Spivak, D. E. Nikitopoulos, R. L. McCarley and S. A. Soper, *Langmuir*, 2011, **27**, 7949–7957.
24 M. Hashimoto, S. S. Shevkoplyas, B. Zasońska, T. Szymborski, P. Garstecki and G. M. Whitesides, *Small*, 2008, **4**, 1795–1805.
25 J. Hong, M. Choi and J. B. Edel, *Lab Chip*, 2010, **10**, 2702–2709.
26 D.-T. Phan and N.-T. Nguyen, *Appl. Phys. Lett.*, 2014, **104**, 084104.
27 V. van Steijn, C. R. Kleijn and M. T. Kreutzer, *Phys. Rev. Lett.*, 2009, **103**, 214501.
28 H. Kinoshita, S. Kaneda, T. Fujii and M. Oshima, *Lab Chip*, 2007, **7**, 338–346.
29 U. Miessner, R. Lindken and J. Westerweel, *Velocity measurements in microscopic two-phase flows by means of micro PIV*, 2008.
30 M. Hein, M. Moskopp and R. Seemann, *Lab Chip*, 2015, **15**, 2879–2886.
31 K. Cheung, S. Gawad and P. Renaud, *Cytometry, Part A*, 2005, **65**, 124–132.
32 E. Du, S. Ha, M. Diez-Silva, M. Dao, S. Suresh and A. P. Chandrakasan, *Lab Chip*, 2013, **13**, 3903–3909.
33 A. J. Eisfeld, G. Neumann and Y. Kawaoka, *Nat. Protoc.*, 2014, **9**, 2663–2681.
34 H. E. Ayliffe, A. B. Frazier and R. Rabbitt, *J. Microelectromech. Syst.*, 1999, **8**, 50–57.
35 T. Sun and H. Morgan, *Microfluid. Nanofluid.*, 2010, **8**, 423–443.
36 H. Morgan, T. Sun, D. Holmes, S. Gawad and N. G. Green, *J. Phys. D: Appl. Phys.*, 2006, **40**, 61.
37 H.-L. Gou, X.-B. Zhang, N. Bao, J.-J. Xu, X.-H. Xia and H.-Y. Chen, *J. Chromatogr. A*, 2011, **1218**, 5725–5729.
38 P. Dak, A. Ebrahimi and M. A. Alam, *Lab Chip*, 2014, **14**, 2469–2479.
39 T. Sun, S. Gawad, N. G. Green and H. Morgan, *J. Phys. D: Appl. Phys.*, 2006, **40**, 1.
40 H. Fricke, *Phys. Rev.*, 1925, **26**, 678–681.
41 H. Fricke, *Phys. Rev.*, 1925, **26**, 682–687.
42 L.-S. Jang and M.-H. Wang, *Biomed. Microdevices*, 2007, **9**, 737–743.